Electronic Supplementary Material (ESI) for Dalton Transactions

Electronic Supplementary Information for

Dinuclear mixed-valence $Co^{III}Co^{II}$ complexes derived from a macrocyclic ligand: unique example of a $Co^{III}Co^{II}$ complex showing catecholase activity

Samit Majumder,*[,a] Suraj Mondal,[a] Pascale Lemoine[b] and Sasankasekhar Mohanta*[,a]

Table S1 The molar conductance values (ohm^{-1} cm^{-1} mol^{-1} l) at 298 K for **1**–**3** in different solvents.

Solvent	1	2	3
DMF	8	17	75
MeCN	2.9	40	158
MeOH	10	–	–

Table S2 Selected bond lengths (Å) and angles (º) for $[Co^{III}Co^{II}L(N_3)_3]\cdot CH_3CN$ (**1**).

Co(1)–O(1)	1.929(3)	Co(2)–O(1)	2.076(3)
Co(1)–O(2)	1.933(3)	Co(2)–O(2)	2.042(3)
Co(1)–N(1)	1.915(3)	Co(2)–N(3)	2.059(3)
Co(1)–N(2)	1.911(3)	Co(2)–N(4)	2.039(4)
Co(1)–N(5)	1.969(3)	Co(2)–N(11)	1.978(4)
Co(1)–N(8)	1.947(4)	Co(1)···Co(2)	3.064
N(5)–Co(1)–N(8)	178.30(15)	O(1)–Co(2)–N(3)	150.01(12)
O(1)–Co(1)–N(2)	173.20(13)	O(2)–Co(2)–N(4)	145.53(12)
O(2)–Co(1)–N(1)	172.89(13)	N(11)–Co(2)–O(1)	109.35(14)
N(5)–Co(1)–O(1)	90.81(13)	N(11)–Co(2)–O(2)	113.05(15)
N(5)–Co(1)–O(2)	90.43(13)	N(11)–Co(2)–N(3)	100.19(15)
N(5)–Co(1)–N(1)	88.87(14)	N(11)–Co(2)–N(4)	100.95(16)
N(5)–Co(1)–N(2)	89.57(14)	O(1)–Co(2)–O(2)	75.39(10)
N(8)–Co(1)–O(1)	89.36(13)	O(1)–Co(2)–N(4)	88.51(12)
N(8)–Co(1)–O(2)	91.26(13)	O(2)–Co(2)–N(3)	88.62(12)
N(8)–Co(1)–N(1)	89.44(14)	N(3)–Co(2)–N(4)	90.94(14)
N(8)–Co(1)–N(2)	90.46(15)	Co(1)–O(1)–Co(2)	99.74(12)
O(1)–Co(1)–O(2)	81.41(11)	Co(1)–O(2)–Co(2)	100.82(12)
O(1)–Co(1)–N(1)	91.53(13)		
O(2)–Co(1)–N(2)	91.80(13)		
N(1)–Co(1)–N(2)	95.27(14)		

Table S3 Selected bond lengths (Å) and angles (º) for $[Co^{III}Co^{II}L(OCN)_3]\cdot CH_3CN$ (**2**).

Co(1)–O(1)	1.945(4)	Co(2)–O(1)	2.074(4)
Co(1)–O(2)	1.930(4)	Co(2)–O(2)	2.036(4)
Co(1)–N(1)	1.919(5)	Co(2)–N(3)	2.055(5)
Co(1)–N(2)	1.910(5)	Co(2)–N(4)	2.068(5)
Co(1)–N(5)	1.700(12)	Co(2)–N(7)	1.950(7)
Co(1)–N(6)	1.945(6)	Co(1)···Co(2)	3.067
N(5)–Co(1)–N(6)	178.7(3)	O(1)–Co(2)–N(3)	139.91(19)
O(1)–Co(1)–N(2)	171.82(19)	O(2)–Co(2)–N(4)	149.34(19)
O(2)–Co(1)–N(1)	172.84(19)	N(7)–Co(2)–O(1)	122.4(2)
N(5)–Co(1)–O(1)	89.0(2)	N(7)–Co(2)–O(2)	107.0(2)
N(5)–Co(1)–O(2)	92.6(2)	N(7)–Co(2)–N(3)	97.3(2)
N(5)–Co(1)–N(1)	89.3(2)	N(7)–Co(2)–N(4)	103.4(2)
N(5)–Co(1)–N(2)	90.5(2)	O(1)–Co(2)–O(2)	74.97(15)
N(6)–Co(1)–O(1)	89.9(2)	O(1)–Co(2)–N(4)	85.62(19)
N(6)–Co(1)–O(2)	88.0(2)	O(2)–Co(2)–N(3)	89.04(17)
N(6)–Co(1)–N(1)	90.0(2)	N(3)–Co(2)–N(4)	91.0(2)
N(6)–Co(1)–N(2)	90.6(2)	Co(1)–O(1)–Co(2)	99.36(17)
O(1)–Co(1)–O(2)	80.38(16)	Co(1)–O(2)–Co(2)	101.20(17)
O(1)–Co(1)–N(1)	92.74(19)		
O(2)–Co(1)–N(2)	91.48(18)		
N(1)–Co(1)–N(2)	95.4(2)		

Table S4 Selected bond lengths (Å) and angles (º) for $[Co^{III}Co^{II}L(\mu\text{-}CH_3COO)_2](ClO_4)$ (**3**).

Co(1)–O(1)	1.923(2)	Co(2)–O(1)	2.020(2)
Co(1)–O(2)	1.922(2)	Co(2)–O(2)	2.018(2)
Co(1)–N(1)	1.934(3)	Co(2)–N(3)	2.016(3)
Co(1)–N(2)	1.931(3)	Co(2)–N(4)	2.017(3)
Co(1)–O(4)	1.933(2)	Co(2)–O(3)	2.279(2)
Co(1)–O(6)	1.909(2)	Co(2)–O(5)	2.100(3)
Co(1)···Co(2)	2.8557(8)		
O(2)–Co(1)–N(1)	177.85(10)	O(3)–Co(2)–O(5)	151.86(9)
O(1)–Co(1)–N(2)	177.22(10)	O(1)–Co(2)–N(3)	169.17(10)
O(4)–Co(1)–O(6)	176.18(10)	O(2)–Co(2)–N(4)	169.60(10)
O(4)–Co(1)–O(1)	89.64(8)	O(3)–Co(2)–O(1)	77.82(9)
O(4)–Co(1)–O(2)	89.55(9)	O(3)–Co(2)–O(2)	78.69(8)
O(4)–Co(1)–N(1)	90.03(11)	O(3)–Co(2)–N(3)	92.26(10)
O(4)–Co(1)–N(2)	90.64(10)	O(3)–Co(2)–N(4)	92.17(10)
O(6)–Co(1)–O(1)	87.25(9)	O(5)–Co(2)–O(1)	80.53(9)
O(6)–Co(1)–O(2)	88.22(10)	O(5)–Co(2)–O(2)	81.55(9)
O(6)–Co(1)–N(1)	92.08(12)	O(5)–Co(2)–N(3)	107.39(12)
O(6)–Co(1)–N(2)	92.36(11)	O(5)–Co(2)–N(4)	105.16(10)
N(1)–Co(1)–O(1)	88.04(10)	O(1)–Co(2)–O(2)	84.50(8)
O(2)–Co(1)–O(1)	89.85(8)	O(1)–Co(2)–N(4)	88.74(10)
O(2)–Co(1)–N(2)	87.39(10)	O(2)–Co(2)–N(3)	89.32(9)
N(1)–Co(1)–N(2)	94.72(12)	N(3)–Co(2)–N(4)	96.06(11)
Co(1)–O(1)–Co(2)	92.77(8)		
Co(1)–O(2)–Co(2)	92.87(8)		

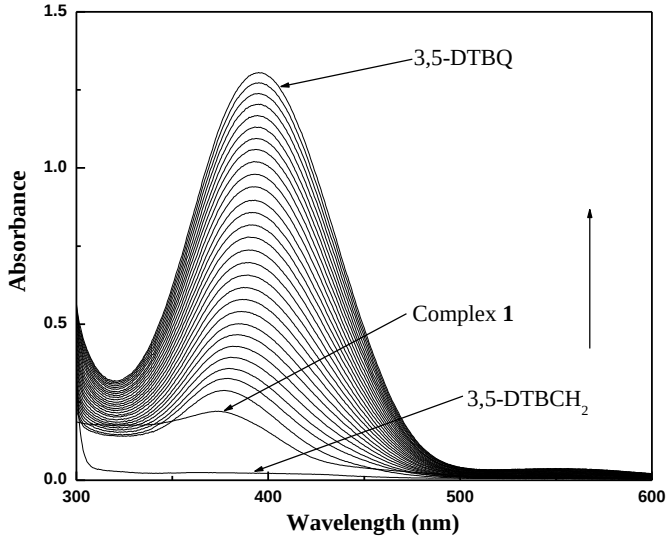

Fig. S1 The spectral profile showing the increase of quinone band at 400 nm after the addition of 100 fold of 3,5-DTBCH$_2$ to a solution containing complex [Co^{III}Co^{II}L(N$_3$)$_3$]·CH$_3$CN (**1**) (0.25×10^{-4} M) in MeOH. The spectra were recorded after each 5 min.

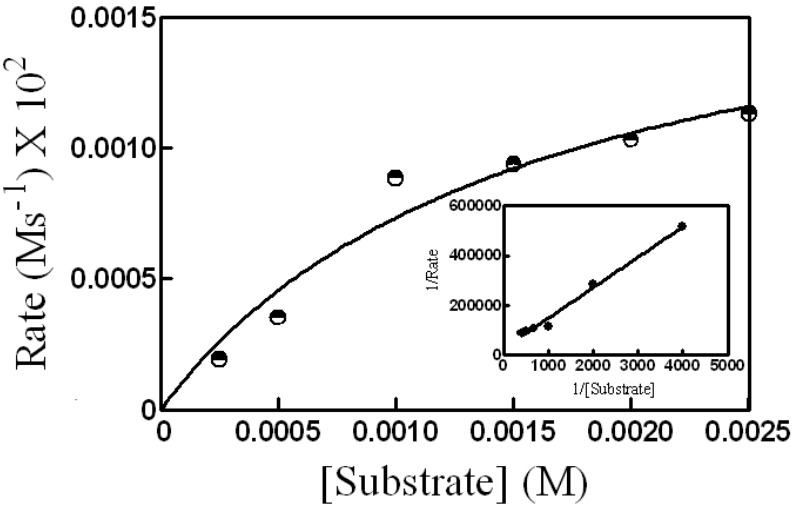

Fig. S2 Initial rates versus substrate concentration for the 3,5-DTBCH$_2$→3,5-DTBQ oxidation reaction catalyzed by complex [Co^{III}Co^{II}L(N$_3$)$_3$]·CH$_3$CN (**1**) in methanol. Inset shows Lineweaver-Burk plot. Symbols and solid lines represent the observed and simulated profiles, respectively.

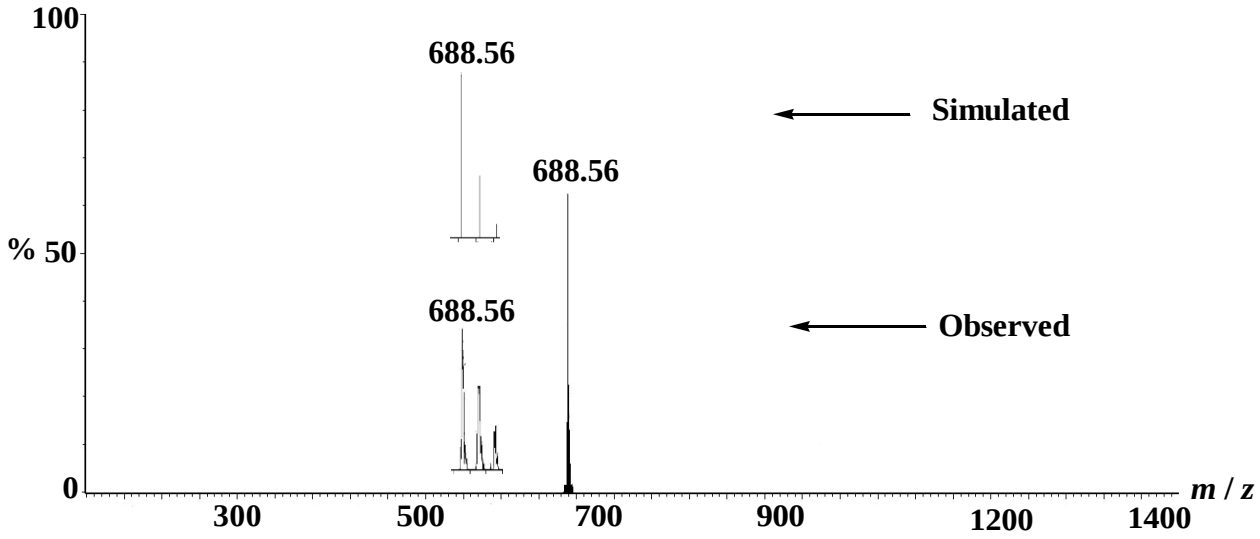

Fig. S3 Electrospray mass spectrum (ESI-MS positive) of $[Co^{III}Co^{II}L(OCN)_3]\cdot CH_3CN$ (**2**) in acetonitrile showing observed and simulated isotopic distribution pattern.

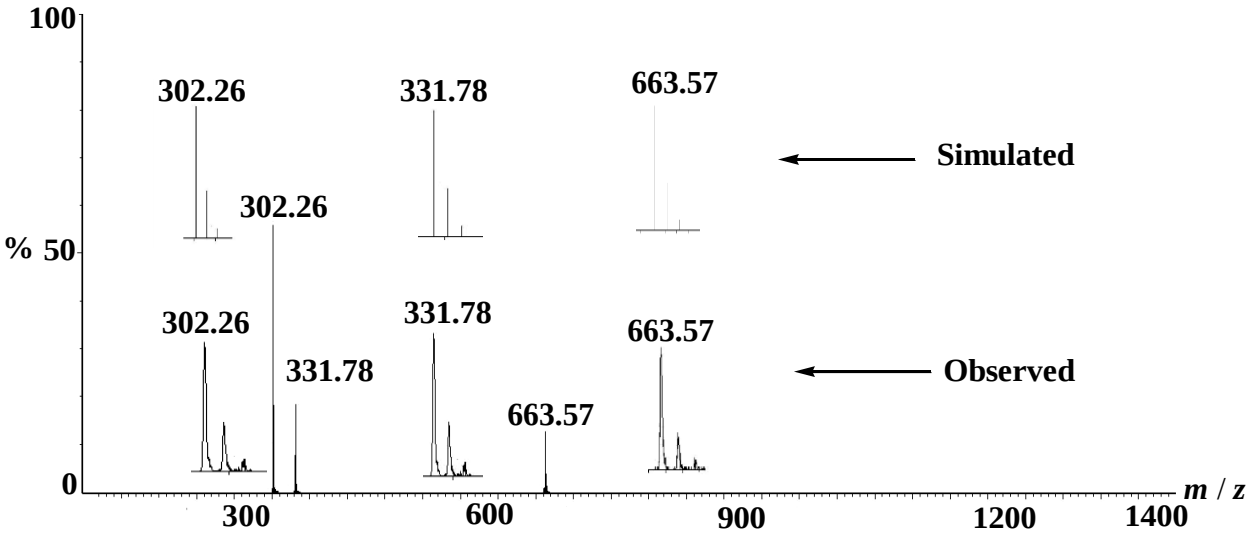

Fig. S4 Electrospray mass spectrum (ESI-MS positive) of $[Co^{III}Co^{II}L(\mu\text{-}CH_3COO)_2](ClO_4)$ (**3**) in acetonitrile showing observed and simulated isotopic distribution pattern.